Advances in Aerodynamics

RESEARCH Open Access

# A symmetry-based length model for characterizing the hypersonic boundary layer transition on a slender cone at moderate incidence

Wei-Tao Bi[1,2], Zhou Wei[1,3,4], Ke-Xin Zheng[1] and Zhen-Su She[1*]

*Correspondence: she@pku.edu.cn
[1]State Key Laboratory for Turbulence and Complex Systems and Department of Mechanics and Engineering Science, College of Engineering, Peking University, Beijing 100871, China
Full list of author information is available at the end of the article

**Abstract**

The hypersonic boundary layer (HBL) transition on a slender cone at moderate incidence is studied via a symmetry-based length model: the SED-SL model. The SED-SL specifies an analytic stress length function (which defines the eddy viscosity) describing a physically sound two-dimensional multi-regime structure of transitional boundary layer. Previous studies showed accurate predictions, especially on the drag coefficient, by the SED-SL for airfoil flows at different subsonic Mach numbers, Reynolds numbers and angles of attack. Here, the SED-SL is extended to compute the hypersonic heat transfer on a 7° half-angle straight cone at Mach numbers 6 and 7 and angles of attack from 0° to 6°. It is shown that a proper setting of the multi-regime structure with three parameters (i.e. a transition center, an after-transition near-wall eddy length, and a transition width quantifying transition overshoot) yields an accurate description of the surface heat fluxes measured in wind tunnels. Uniformly good agreements between simulations and measurements are obtained from windward to leeward side of the cone, implying the validity of the multi-regime description of the transition independent of instability mechanisms. It is concluded that a unified description for the HBL transition of cone is found, and might offer a basis for developing a new transition model that is simultaneously of computational simplicity, sound physics and greater accuracy.

**Keywords:** Hypersonic boundary layer transition, Transition model, Cone, Heat flux

## 1 Introduction

Hypersonic boundary layer (HBL) transition has a crucial impact on the performance of high-speed flying vehicles and has been the focus of many theoretical, experimental and numerical studies during the past several decades [1]. Compared to low-speed flows, HBL transition is subjected to more instability mechanisms and more transition-influential factors [2, 3]. Anderson [4] has concluded that the transition onset Reynolds number of HBL depends on nearly twenty factors, in general. Formulating a model to describe the effects of the many factors has been a long-lasting research target. However,

few results are satisfactory, owing to the complexity from the interplay of multiple factors [2] and from the variation of influential pattern in a wide factor range (e.g. for the nose-tip bluntness effect [5]). Since nearly all transition models include a correlation equation to define the transition onset location [6, 7], which is poorly predicted in general, the existing models usually give insufficient and even undetermined prediction accuracies [8, 9]. Furthermore, HBLs are generally governed by different instability mechanisms on different surface areas [1, 10, 11], which results in enormous complexities in modeling and simulating HBL transitions [12, 13]. The status calls for a reflection: whether one should always rely on a correct description of the transition mechanism for the foundation of a transition model, or perhaps might discover a universal principle governing transitional boundary layers, and work out a more efficient transition model. Here we take the latter perspective and attempt to develop a new approach.

To begin with, we propose a notion of "similarity structure" of boundary layer, which ensures a similarity of the flow for varying Reynolds number (*Re*), Mach number (*Ma*), etc. We further introduce a notion of "order function" as the similarity variable to display the right symmetry of the similarity structure. Specifically, for boundary layers, the most important symmetry is the symmetry under a dilation transformation from the wall in the wall-normal direction and that from the leading edge in the streamwise direction. And the similarity variable is a (stress) length (SL) that characterizes the size of eddies most relevant to the momentum transport (so as to define the eddy viscosity). In the so-called structural ensemble dynamics (SED) theory [14], it has been identified that a wall-normally four-layer structure (corresponding to the viscous sublayer, buffer layer, log-layer and bulk flow) is the similarity structure of turbulent boundary layer (TBL). And its dilation symmetry is expressed by the SL function with a unique scaling law with the wall distance within each layer, as well as a universal scaling transition between adjacent layers, which have been derived from a novel Lie-group analysis of the momentum and energy balance equations [14, 15], and validated in detail for the canonical (i.e. zero-pressure-gradient flat-plate) TBL [14]. As a consequence, the mean-flow profiles of the canonical TBL have been predicted, for the first time, over the whole boundary layer thickness and for all *Re*, at an unprecedented accuracy compared to direct numerical simulation (DNS) and experimental data [14, 16, 17].

More recently, a streamwise three-layer structure (corresponding to the laminar, transitional and fully-developed TBL states, respectively) was suggested for the SL function to describe transitional boundary layers, which yielded a new algebraic transition model called SED-SL [18]. Application of the SED-SL to several airfoil flows (e.g. NACA0012 and RAE2822) at different subsonic *Ma*, *Re* and angles of attack (*AoA*), yielded an unprecedented accuracy (up to a few counts) in the drag prediction [19], indicating the validity of the concept of the similarity structure and pointing out an interesting new direction for turbulence model construction. It is interesting to know whether or not this symmetry-based model can capture the universal features of transition processes, whose parameterization might show more clear dependency on the influential factors, without involving specific instability mechanism that causes the transition. We present here a preliminary study to apply the SED-SL to the HBL transition over a straight cone with an *AoA*, to further validate the merit of the model.

In the following, we employ the SED-SL to compute the transitional flows on a 7° half-angle straight cone at *Ma* 6 and 7 and *AoA* from 0° to 6°. It is shown that, by properly

setting the two-dimensional, multi-regime structure of the HBL over the cone surface through only three parameters of clear physical meaning (i.e. a transition center, an after-transition near-wall eddy length, and a transition width quantifying transition overshoot), the SED-SL correctly reproduces the heat flux distribution on the whole cone surface, in excellent agreement with the wind tunnel data. We demonstrate a simple adaptation of the SED-SL to different flow parameters (e.g. *Ma*, *AoA*, free-stream disturbances), and to different instability mechanisms (which vary with *AoA* and the circumferential angle of the cone). Thus, we have proposed a unified description for the HBL transition under the change of several influential factors and transition mechanisms. With future studies to determine the variations of the three physical parameters with the surface geometry and flow conditions, the SED-SL has a potential to lead a new generation of transition model that is simultaneously of computational simplicity, sound physics and greater accuracy.

The paper is organized as follows. Section 2 describes the SED-SL model and the computational setup. Section 3 presents the results of computation, which validate our predictions for different flow cases. Section 4 is devoted to discussion and conclusion.

## 2 Theory

In the Favre RANS approach, the conservation equations of mass, momentum and energy, under the thin-layer and Boussinesq approximations and assuming constant turbulent Prandtl number, are written as follows [12]:

$$\frac{\partial \bar{\rho}}{\partial t} + \frac{\partial}{\partial x_j}\left(\bar{\rho}\tilde{U}_j\right) = 0, \tag{1}$$

$$\frac{\partial \bar{\rho}\tilde{U}_i}{\partial t} + \frac{\partial}{\partial x_j}\left(\bar{\rho}\tilde{U}_i\tilde{U}_j\right) = -\frac{\partial \bar{P}}{\partial x_i} + \frac{\partial \bar{\sigma}_{ij}}{\partial x_j}, \tag{2}$$

$$\frac{\partial \bar{\rho}\tilde{E}}{\partial t} + \frac{\partial}{\partial x_j}\left(\bar{\rho}\tilde{U}_j\bar{H}\right) = \frac{\partial}{\partial x_j}\left(\tilde{U}_i\bar{\sigma}_{ij}\right) + \frac{\partial}{\partial x_j}\left[C_p\left(\frac{\bar{\mu}}{Pr} + \frac{\mu_t}{Pr_t}\right)\frac{\partial \tilde{T}}{\partial x_j}\right], \tag{3}$$

where overbar denotes Reynolds averaging and tilde denotes Favre averaging; $\rho$ is fluid density, $U_j$ is the $j$-th component of velocity and $x_j$ represents the Cartesian coordinate. $P = \rho RT$ is the static pressure ($R$ is the gas constant) and total entropy $\bar{H} = \tilde{E} + \bar{P}/\bar{\rho}$, where total energy $E = C_v T + K$ with $C_v$ the specific heat at constant volume, $T$ the static temperature and $K$ the kinetic energy of the flow $\left(K = \frac{1}{2}U_k U_k\right)$. The molecular Prandtl number $Pr$ is 0.72, and the turbulent Prandtl number $Pr_t$ is set to 0.9. The stress $\bar{\sigma}_{ij}$ is expressed by using the Boussinesq approximation as follows:

$$\bar{\sigma}_{ij} = 2\left(\bar{\mu} + \mu_t\right)\left(\tilde{S}_{ij} - \frac{1}{3}\tilde{S}_{kk}\delta_{ij}\right), \tag{4}$$

where $S_{ij} = \frac{1}{2}\left(\frac{\partial U_i}{\partial x_j} + \frac{\partial U_j}{\partial x_i}\right)$ is the strain rate tensor. The molecular viscosity $\mu$ is computed by using the Sutherland law: $\frac{\mu}{\mu_\infty} = \frac{1+\mathrm{T}_s/T_\infty}{T/T_\infty+T_s/T_\infty}\left(\frac{T}{T_\infty}\right)^{3/2}$, where $T_S = 110.4(\mathrm{K})$ and subscript $\infty$ indicates the free-stream property. The turbulent viscosity $\mu_t$ has to be modeled.

### 2.1 The SED-SL transition model

The SED theory has extended the classical mixing length concept [20] to multiple Reynolds stress lengths to describe both the Reynolds shear stresses and the Reynolds

normal stresses [15]. The Reynolds shear stress length $\ell_{12}$ in a compressible TBL is defined as:

$$\ell_{12} = \frac{\sqrt{-\widetilde{u''v''}}}{\partial_y \tilde{U}}, \tag{5}$$

where $\tilde{U}$ is the streamwise mean velocity, $u''$ and $v''$ are the Favre fluctuations of the streamwise and wall-normal velocity components, respectively. $\ell_{12}$ has been interpreted as the characteristic size of eddies responsible for the wall-normal turbulent transport of momentum. It is applied for expressing $\mu_t$ of TBL in the SED-SL model as follows [17–19]:

$$\mu_t = \bar{\rho}\ell_{12}^2 |\tilde{\omega}|, \tag{6}$$

where $\tilde{\omega} = \partial_y \tilde{U} - \partial_x \tilde{V}$, following the same convention as in the Baldwin-Lomax model [21].

The SED theory predicts that the stress length $\ell_{12}$ possesses a multilayer form in fully-developed TBL [14, 15]:

$$\ell_{12}^+ = \ell_{12}^{+inner}\left(y^+\right) \times \ell_{12}^{+outer}(r), \tag{7}$$

$$\ell_{12}^{+inner}\left(y^+\right) = \ell_0^+ \left(\frac{y^+}{9.7}\right)^{3/2} \left[1 + \left(\frac{y^+}{9.7}\right)^4\right]^{1/8} \left[1 + \left(\frac{y^+}{y_{buf}^+}\right)^4\right]^{-1/4}, \tag{8}$$

$$\ell_{12}^{+outer}(r) = \frac{\left(1 - r^4\right)}{4\left(1 - r\right)}, \tag{9}$$

where $y^+$ is the distance from the wall in the wall unit (i.e. $y^+ = yu_\tau/\bar{\nu}_w$, $\nu$ is the kinematic viscosity, $u_\tau$ is the friction velocity: $u_\tau = \sqrt{\bar{\mu}_w \frac{d\tilde{U}}{dy}\Big|_w / \bar{\rho}_w}$, and subscript $w$ denotes wall value), $y_{buf}^+$ is the thickness of the buffer layer, $\ell_0^+ = 9.7^2\kappa/y_{buf}^+$ is the near-wall eddy length, and $\kappa$ is the Karman constant. $r = 1 - y/\delta$ is the outer coordinate, being the distance (to the wall) from the outer dilation center (at $\delta$) of the TBL. In the current model, $\delta$ is evaluated following the Baldwin-Lomax model [21] by

$$\delta = \frac{y_{\max}}{0.3}, \tag{10}$$

where $y_{\max} = y\left(\max\left(\ell_{12}^{+inner}|\tilde{\omega}|\right)\right)$. Eq.(7)-Eq.(9) describe a wall-normally four-layer structure for the canonical TBL, including the viscous sublayer (with thickness 9.7 and power law of $\ell_{12}^+ \propto y^{+3/2}$), buffer layer (with thickness $y_{buf}^+$ and power law of $\ell_{12}^+ \propto y^{+2}$), log-layer and bulk/wake flow (with the $1 - r^4$ structure); it is easy to verify that for $y^+ \gg y_{buf}^+$ and $r \approx 1$ in Eq.(7), i.e. in the matching region between the inner and outer regimes of TBL, one obtains the celebrated linear law $\ell_{12}^+ = \kappa y^+$ of Prandtl [20].

For the canonical TBL the SED asserts that $y_{buf}^+$ is about 41, and $\kappa$, 0.45, thus $\ell_0^+$ is about 1.03. Consequently there is no free parameter in Eq.(7)-Eq.(9), but adequate to accurately predict the whole mean velocity profile of canonical TBL at all (above moderate) *Re* [14]. As to non-canonical TBLs, the above four-layer structure may be deformed by the influential factors (such as pressure gradient) and evolve spatially. A crucial assumption of the SED is that, because the wall constraint remains the dominant effect, the deformation is only finite, slow and continuous, such that it can be described with variable multi-layer structure parameters. Two parameters have been identified to be crucial: $\ell_0^+$ and $y_{buf}^+$,

which determine the global size and location of the strongest eddies (which are vulnerable to environmental variation) and thus characterise the major deformation of the boundary layer. The above assumption has been validated for a series of non-canonical TBLs, in particular, the transitional boundary layer (TrBL) [18, 19].

To describe the TrBL, Xiao and She [18] have proposed a two-dimensional multi-regime structure by postulating a streamwise multilayer dilation with respect to the leading edge (i.e. $x = 0$) for $\ell_0^+$ and $y_{buf}^+$. Here, for the transitional HBL of cone, they are written as follows:

$$\ell_0^+ = \ell_{0\infty}^+ \left(\frac{x}{x^*}\right)^5 \left[1 + \left(\frac{x}{x^*}\right)^{10}\right]^{-1.5} \left[1 + \left(\frac{x}{\beta_l x^*}\right)^{10}\right] \beta_l^{10}, \tag{11}$$

$$y_{buf}^+ = 41 \left(\frac{x}{x^*}\right)^{5.5} \left[1 + \left(\frac{x}{x^*}\right)^{10}\right]^{-5.5/10}, \tag{12}$$

in which three transition parameters are introduced. $x^*$ is called the transition center, being a newly-identified indicator for the transition location that is believed superior in physics than the conventional transition onset location [18]. $x^*$ requires further modeling and remains an adjustable model parameter in the present study. $\ell_{0\infty}^+$ characterises the near-wall eddy size of the fully-developed TBL; it determines the skin friction and surface heat flux after the transition. $\ell_{0\infty}^+$ depends on pressure gradient, $Ma$ and wall temperature ($T_w$), etc. [19]. For not-far-from adiabatic TrBL with less than moderate pressure gradient, such as the current cone flows, $\ell_{0\infty}^+$ is around unity, i.e. the canonical TBL value; for hypersonic flow over significantly cooled wall, it can be substantially smaller than unity owing to the strong squeezing effect of very large $Ma$ and very small $T_w$ on the eddy size. $\beta_l \geq 1$ is a coefficient that quantifies the strength of the transition overshoot (a phenomenon that the skin-friction coefficient and Stanton number at around the transition end considerably surpass their TBL values at the same Reynolds number). It is the ratio of the location where the transition starts to relax to the fully-developed TBL to the location of the transition center, thus it (when larger than unity) defines a unique transition regime between the laminar and fully-turbulent regimes. The larger the $\beta$, the wider the transition regime, the stronger the transition overshoot, and the higher the peak heat flux. When $\beta = 1$, no transition regime or transition overshoot appears. For most by-pass transitions, the typical value of $\beta$ is about 1.1.

Note that the scaling exponents 5 in Eq. (11) and 5.5 in Eq. (12) are empirical parameters determined previously by using experimental data of a series of bypass transitions [18, 19]. They quantify the streamwise establishment of the wall-normally four-layer structure of TBL during the transition process. Or, frankly speaking, they quantify the transition speed. For most bypass transitions subjected to free-stream disturbances in conventional wind tunnels, the current setting is adequate. In the DNS cases, however, the transition seems to be much quicker than that in the experiment and larger scaling exponents are required to gain an accurate description. See the discussion in [19].

Here we apply the above model to investigate the hypersonic transitional flows over straight cones at moderate $AoA$. As is presented, varying the three model parameters yields accurate descriptions of a substantial variety of surface heat flux distributions in the HBL transition of straight cone. A note about the computation is that, the streamwise coordinate $x$ in Eqs. (11) and (12) is approximated by the axial coordinate of the

cone (which is also denoted by $x$ with $x = 0$ being the cone nose tip) for computational simplicity, which affects very little at moderate *AoA*.

### 2.2 Numerical implementation

The RANS equations closed by the SED-SL model were solved by using the CFL3D, which was developed in the early 1980s in the Computational Fluids Laboratory at NASA Langley Research Center, and has been used to support numerous NASA programs since then and continues to be used today, particularly for validation and verification of newly developed turbulence models. The current SED-SL code was developed based on the code of the B-L model in CFL3D, considering their apparent similarity.

Three sets of grid have been tested for the 7° half-angle cone. Grid one has a uniform mesh with grid number 31 in the circumferential direction (from 0° to 180°, i.e. a half-model simulation), an increasingly coarsening mesh with grid number 173 in the axial direction, and a stretching mesh with grid number 131 in the wall normal direction. The physical dimension of the grid is: 1275 mm of cone length, 64 mm of radius in the front plane and 1325 mm of radius in the end plane of the cone. It has been verified that the first wall-normal mesh has a dimension of $y^+ < 0.7$ over the whole cone surface for all the investigated cases. Grid two is doubled in the circumferential direction, and grid three is doubled in both the circumferential and axial directions, for testing grid convergence.

The boundary conditions are set as the following. The free stream boundary condition is used for the inflow. The isothermal, no-slip, solid-wall boundary condition is employed on the cone surface. Since we have conducted a half-model simulation, the symmetry condition is applied on the symmetry plane. Finally, the extrapolation condition is used for the outflow.

As to the numerical algorithms, an implicit approximate-factorization method is applied for time advancing. The viscous fluxes are computed with the second-order central differences, and the inviscid fluxes are computed with the upwind flux-difference-splitting method. The RANS equations are solved in parallel on a workstation with 16 CPU cores.

The experimental data sets used for validation are listed in Table 1. They are selected from the very recent measurements on the surface heat flux and/or surface temperature of 7° half-angle straight cones at moderate *AoA*, all covering a major portion of cone surface with high measurement accuracy. The first experiment was conducted by Willems et al. [22] in the hypersonic wind tunnel (H2K) of the German Aerospace Center (GAC) in Cologne. Surface temperatures and heat fluxes were measured by means of quantitative infrared thermography for the whole cone surface. The second experiment was performed by Chen et al. [23] in the Φ1m Hypersonic Wind Tunnel of the China Aerodynamics Research and Development Center (CARDC). Only surface temperature was measured for the windward and leeward cone surfaces by quantitative infrared thermography. In Table 1, $R_N$ denotes the cone nose-tip radii, $P_0$ is the total pressure, $T_0$ is the

**Table 1** The flow parameters of the test cases

| Case | $Re_\infty(\times 10^7 m^{-1})$ | $Ma_\infty$ | $P_0$(MPa) | $T_0$(K) | $T_w$(K) | *AoA*(°) | $R_N$(mm) |
|---|---|---|---|---|---|---|---|
| GAC-0,6 | 0.911 | 7 | 2.288 | 601.4 | 300 | 0,6 | 1.6 |
| CARDC-0,2,4,6 | 1.0 | 6 | 1.1 | 474 | 300 | 0,2,4,6 | 0.05 |

total temperature, and $T_w$ is the cone surface temperature set in the current numerical simulation.

## 3 Result

Before presenting the results, the effects of the grid and isothermal wall condition on the simulation results have been assessed. For the grid convergence, it has been found that grid one is adequate for $AoA$ no more than 4°, but grid two has to be used for accurately calculating the surface heat flux around the leeward center of the cone at $AoA = 6°$, because of the strong streamwise vortices there. The other issue is about the isothermal wall condition applied in the simulation. In the GAC experiment, the cone surface temperature was measured by quantitative infrared thermography and the surface heat flux was derived accordingly based on a heat-transfer model. One finds in [22] that for the GAC cases the surface temperature in the turbulent region is clearly larger than that in the laminar region, and the temperature difference can be as large as 60 K for the GAC-6 case, which is about 10% of the stagnation temperature (whereas in the CARDC-6 case, only about 1%). So the cone surface is not actually isothermal as the setting of the numerical simulation. We have assessed the effects of the isothermal wall condition on the surface heat flux distribution by increasing the wall temperature from 300 K to 340 K in the GAC-6 case. Indeed, about 15% decrease of heat flux can be found in some locations. Neglecting such a discrepancy, the isothermal wall condition is utilized for simplicity in the current studies.

Validation of the model is conducted by comparing the surface heat fluxes. The dimensionless heat flux $C_h$ (or the Stanton number $St$) is defined as:

$$C_h = St = \frac{k_w \frac{\partial T}{\partial y}|_w}{\rho_\infty U_\infty C_p (T_r - T_w)}, \tag{13}$$

where $T_r = T_\infty \left(1 + r(\gamma - 1) {Ma_\infty}^2/2\right)$ [24] with $\gamma = 1.4$, $r = \sqrt{Pr}$ [25] (i.e. the laminar value. Changing to the turbulent value of $r = Pr^{1/3}$ leads to a change of $St$ smaller than a few percent.), $k$ is the thermal conductivity, and $C_p$ is the specific heat at constant pressure. The focus on $C_h$ is because of the following. $C_h$ is the most widely measured quantity and the upmost concern in engineering applications. It indicates the location, strength and extension of the transition process, and provides a strong constraint to the flow field: if the TrBL is not correctly simulated, the $C_h$ distribution can hardly be correct.

The current study serves a purpose to validate the SED-SL description of the various hypersonic TrBLs over the cone through the aforementioned three model parameters (i.e. $x^*$, $\ell^+_{0\infty}$, $\beta_l$), which are determined after a prediction-correction procedure: first, setting the parameter values; second, solving the RANS equations with the SED-SL model; third, comparing the numerical prediction with the experimental results and updating the parameters until an accurate prediction is achieved. Note that such a procedure can easily be implemented only because the current model parameters have clear physical meanings and are directly related to the shape of the $C_h$. By continuously repeating this procedure in different sample flow cases, the SED-SL eventually will cover a wide flow regime and gain full prediction capacity for engineering applications.

### 3.1 Simulation of the GAC experiment

Following the above procedure, the three parameters are measured for the GAC and CARDC cases. In the current flows $\ell^{+}_{0\infty}$ is found invariant with *AoA* and the circumferential angle $\theta$, and identical to the canonical TBL value ($\approx 1.0$), which perhaps is because *Ma* is not very large, the cone surface is not very cold, and the pressure gradient is mild. In comparison, $\beta_l$ and especially $Re_{x^*}$ vary with *AoA* and $\theta$, as shown in Fig. 1.

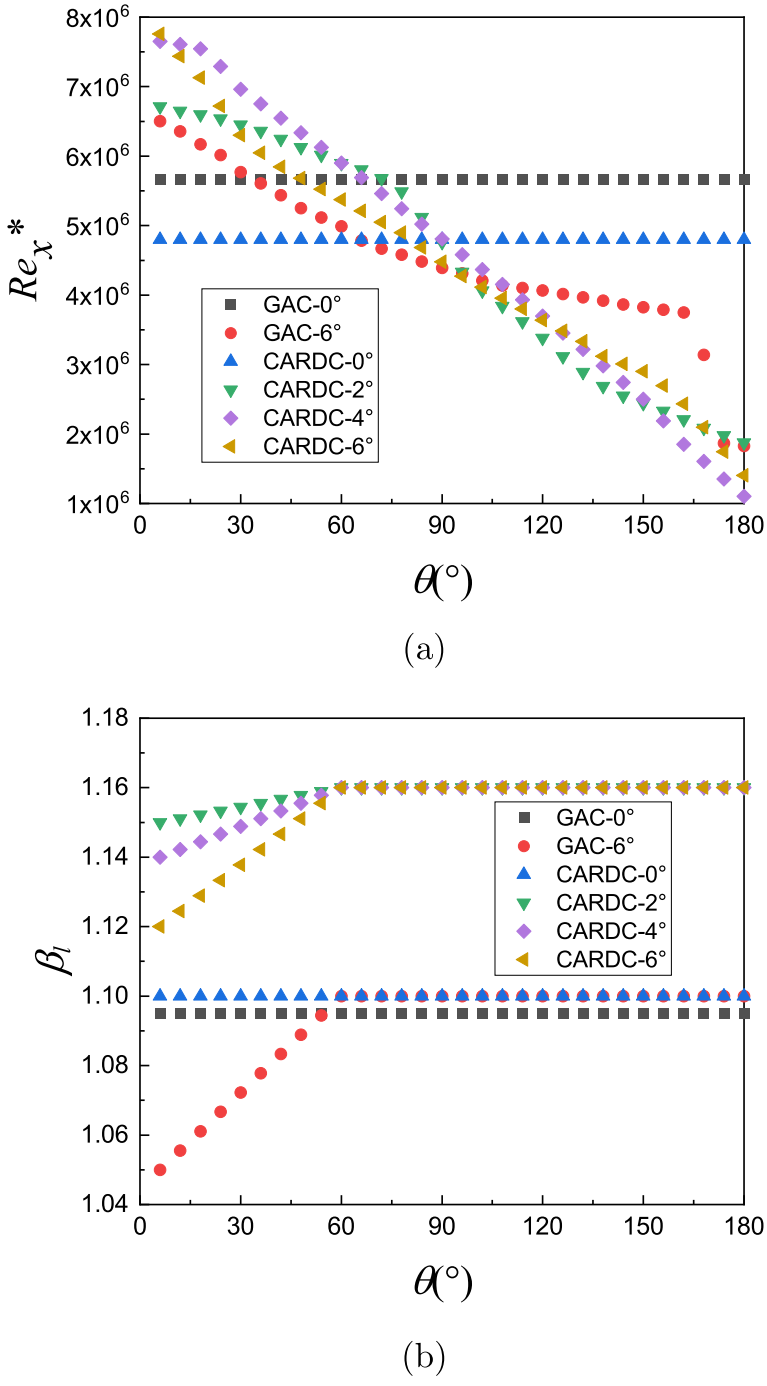


**Fig. 1** Variations of **a** the transition center Reynolds number $Re_{x^*}$ and **b** the transition overshoot strength parameter $\beta_l$ with the circumferential angle $\theta$ for the GAC and CARDC test cases

$Re_{x^*}$ ($= x^* Re_\infty$) is a new indicator of the transition front. At $AoA = 2°$ and 4° of the CARDC cases, $Re_{x^*}$ varies almost linearly with $\theta$ and becomes flattened near $\theta = 0°$ and 180° to adapt to the symmetry condition. At $AoA = 6°$, one finds in Fig. 1a that $Re_{x^*}$ begins to break up into three regions: a windward region with a significantly postponed and rapid changing transition front, a wide cross-flow region with a relatively slowly advancing transition front, and a narrow leeward region with a much earlier transition front. Such a behaviour is more apparent for the GAC-6 case than the CARDC-6 case. The reason for this break-up is likely because of the circumferential variation of the dominant transition mechanism at moderate *AoA* [11]. Indeed, the Mack second mode that governs the whole cone surface at zero incidence shrinks to a portion of the windward region with increasing *AoA*. The cross-flow mode then occupies the main surface of the cone owing to the wide-spread pressure gradient in the circumferential direction, leaving only a narrow leeward region for the streamwise vortex mode, where streamlines converge and form counter-rotating streamwise vortices that promote the transition.

The variation of $\beta_l$ is simpler (Fig. 1b). It is invariant with *AoA* and $\theta$ in the cross-flow and leeward regimes, but decreasing (linearly, in the present empirical setting) with decreasing $\theta$ in the windward region. In the cone windward, $\beta_l$ also decreases with increasing *AoA*, which means that the transition overshoot becomes weak in the cone windward as the *AoA* is increased, owing perhaps to the stronger compressibility there. More studies are needed to clarify this phenomenon. In addition, there is a clear difference regarding the transition overshoot strength between the GAC-6 and CARDC-6 cases. The CARDC-6 cases have much stronger transition overshoots than those of the GAC-6 cases. The reason is unclear, but it may be due to the different free-stream noise levels of the CARDC and GAC wind tunnels [26].

Figure 2 compares the SED-SL computed *St* distribution along the meridian line of the cone surface with the measured one for the GAC-0 case. The simulation excellently agrees with the measurement throughout the whole transition process. Especially, the transition onset location (defined as the location with minimum *St*) and the peak surface heat flux are computed very accurately, whose relative errors are less than 2%.

Figure 2 also includes a comparison between the *St* distribution and the measured surface temperature increment ($\Delta T_w$, with a reference $T_w$ of 300 K) distribution with proper normalization. The reason for this comparison is explained as the following. HBL transition has been more and more frequently diagnosed by quantitative infrared thermography for its high fidelity, wide angle of view and nonintrusion. However, the technique measures only the surface temperature and the heat flux has to be derived accordingly by an algorithm with specific heat transfer assumptions. In the CARDC experiments (and many others), only the surface temperature data are provided. Thus it is interesting to study the relationship between $\Delta T_w$ and *St*, to identify whether or not $\Delta T_w$ can be an acceptable approximation of the surface heat flux. In Fig. 2 one finds that, for the GAC-0 case, by introducing a proportional factor to collapse $\Delta T_w$ with *St* in the laminar region, the rescaled $\Delta T_w$ almost collapses with *St* over the whole TrBL, except a rather limited distinction owing mainly to the discrepancy of the transition onset location. Although this apparent similarity has to be further validated with heat transfer models, it is understandable because the measurements are often conducted with a very short duration, such that $\Delta T_w$ is strongly correlated with the local surface heat flux. Therefore, in the next section, the CARDC data of $\Delta T_w$ are utilized as substitutes for studying the heat flux distributions,

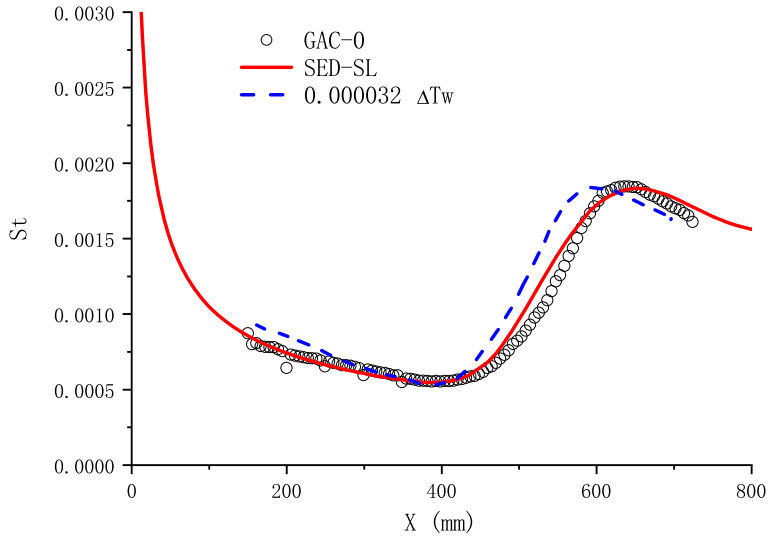


**Fig. 2** The *St* distribution along the meridian line computed by the SED-SL model for the GAC-0 case, compared with the measured *St* distribution and the measured surface temperature increment with appropriate normalization to collapse in the laminar region

which is more convincing considering their temperature increments are much smaller than those of the GAC cases.

Figure 3 compares the SED-SL computed *St* contour with the measured one for the GAC-6 case. The simulation result is almost identical to the measured contour over the whole cone surface. A unique behaviour in the experiment is that, there is an array of distinct, standing cross-flow vortices at around $\theta = 135°$, extending streamwise over a considerably long length with a slight inclination towards the leeward side of the cone. These vortices are stationary, usually occur in a quiet or low-noise environment, and are often induced by surface roughness [10]. The cross-flow vortices disappear suddenly at $\theta < 135°$, which is due to different wind-tunnel runs, as said in [22]. So, it is clear that a large portion of the cone surface is governed by the cross-flow transition, as aforementioned. In a rather narrow range around $\theta = 180°$, the transition onset is significantly earlier, along with a heat flux valley at $\theta = 180°$, which is apparently due to the counter-rotating streamwise vortices. As shown in Fig. 3, the SED-SL simulation reproduces with many details the elaborate distribution of *St* on the cone surface, but does not present the standing cross-flow vortices on the lateral side of the cone.

The reason deserves further discussions. The current model is based on describing the dilation symmetry property of boundary layers, which emerges as a result of the self-organization of a set of turbulent eddies. In the case of a flow dominated by distinct vortices, which often occurs when the disturbances are slight or in a particular form, the flow evolves dynamically with usually discrete characteristic lengths, rather than statistically with continuously-distributed length scales (such that the power law is established). Therefore, it will be more difficult, if not possible, for the SED-SL to describe the flows whose length scales are not fully agitated, e.g. in the early stages of transition in some cases. In the hypersonic transition, such flows could be the stationary cross-flow vortices, or particular development of the Mack second mode that may lead to an additional peak heat flux before transition [27, 28].

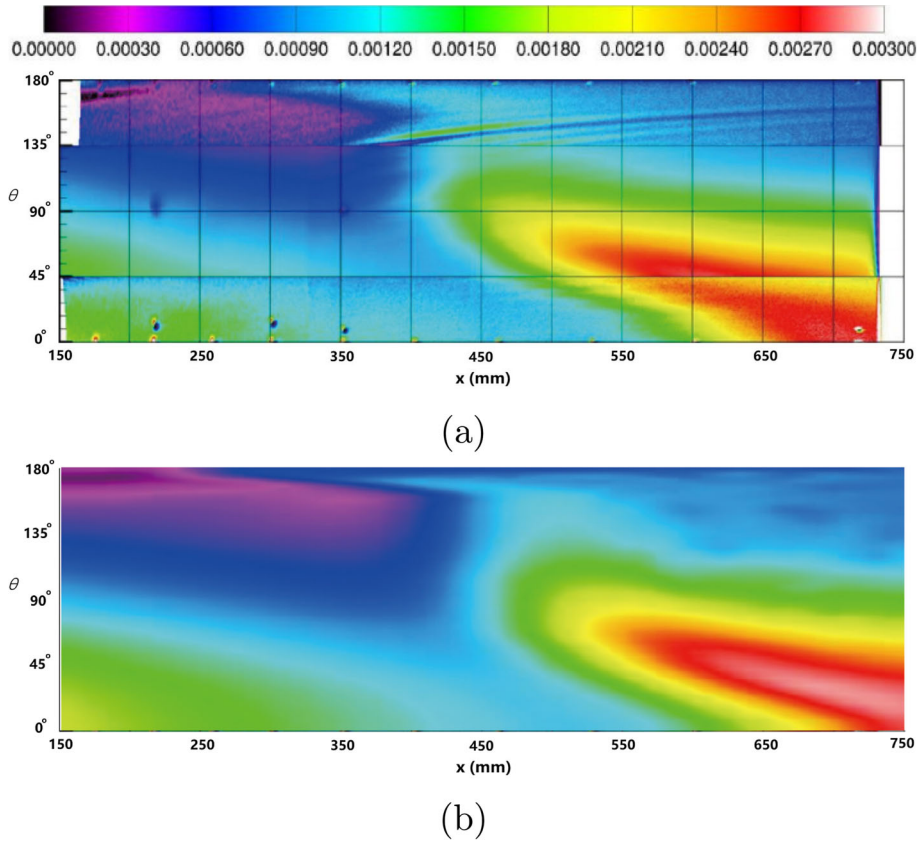


**Fig. 3** The *St* contours **a** measured by Willems et al. [22] and **b** computed by the SED-SL model for the GAC-6 case

More quantitative comparisons are conducted by plotting the SED-SL computed *St* profiles along different meridian lines together with the corresponding measured ones acquired from the experimental contour (i.e. Fig. 3a), which are shown in Fig. 4 for the windward, cross-flow and lee sides, respectively. For all the circumferential angles, the simulated profiles agree excellently with the measured ones over the whole hypersonic TrBLs. The relative errors of the computed transition onset location and peak heat flux are within a few percent, which are prominent if one recalls the current status of the hypersonic transition models (Note that the SED-SL in the current study has not been a transition prediction model as the others).

Let us discuss more about the transition overshoot. Transition overshoot widely occurs in by-pass transitions with strong environmental disturbances. It leads to significant increase of peak surface heat flux in hypersonic flows that affects the thermal protection design. A clear understanding of the overshoot phenomenon is not yet established, which results in the failure of most RANS-based transition models in predicting the peak heat transfer. Qin et al. [29] have used an algebraic intermittency factor to accelerate the development of TBL in the late transition region, such that the overshoot phenomenon is reproduced with a reasonable degree of accuracy. However, Qin et al.'s method is based on the perspective of transition model construction, and its applicability to complex configurations requires further investigations [13]. In the present approach, the transition overshoot is characterized by a single parameter, $\beta_l$, which, if

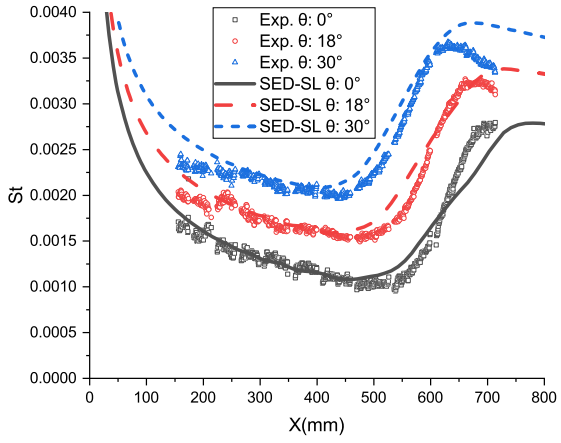


(a)

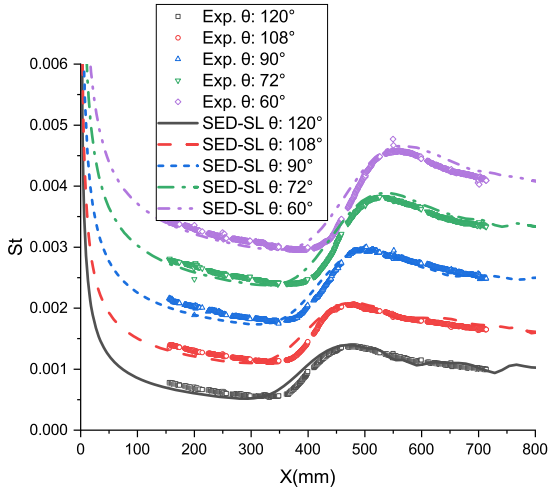


(b)

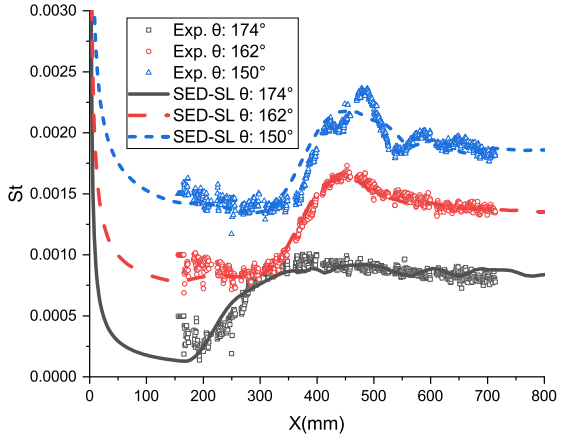


(c)

**Fig. 4** Comparisons between the *St* distributions along the meridian lines measured in experiment [22] and computed by the SED-SL model for **a** the windward surface, **b** the lateral surface, and **c** the leeward surface of the GAC-6 case. The data are vertically translated to be clearly displayed

larger than unity, introduces a streamwise transition layer in between the laminar and full-turbulent flows. In this layer, eddies stimulated upstream by intense disturbances become highly developed, leading to a violent organization that requires a considerable length (quantified by $\beta_l$) to relax eventually to a conventional TBL. This streamwise transition layer mimics the buffer layer (in which the eddies are strong) in the wall-normal direction of TBL, which exists in between the viscous sublayer and the full-developed log-layer and bulk flow [30]. From this point of view, the transition overshoot is a normal phenomenon, and the robustness of $\beta_l$ in depicting various by-pass transitions is understandable.

Now we report the streamwise development of the hypersonic TrBL on the cone surface revealed by the three physical parameters of the SED-SL model. Figure 5 shows the variations of $\ell_0^+$ and $y_{buf}^+$ along different meridian lines for the GAC-6 case. $y_{buf}^+$ denotes the thickness of the buffer layer, i.e. the location of the near-wall coherent structures, which has a crucial impact on the shape of the mean velocity profile, but is difficult to measure in experiments on high-speed boundary layers. In the current setting of the SED-SL model, $y_{buf}^+$ has a streamwise two-layer development that depends only on $x^*$ (see Eq. (12) and Fig. 5b), which can be seen as a first-order approximation. With DNS and possible experimental profile data, the two-layer model of $y_{buf}^+$ can be assessed and refined in the future.

On the other hand, $\ell_0^+$ is more directly relevant to the skin friction and surface heat flux distributions on the cone surface because it determines the magnitude of the stress length and thus the levels of the eddy viscosity and eddy conductivity. As shown in Fig. 5a, $\ell_0^+$ possesses a three-layer streamwise evolution, especially for the cross-flow and leeward sides of the cone (on the lee side $\theta = 174^\circ$ is selected to avoid the heat flux valley), where about 25% overshoot can be found for $\ell_0^+$ compared with the TBL value. At the windward center, the transition overshoot is not apparent as aforementioned. From Fig. 5 one finds that, although the transition mechanisms are very different in the windward, cross-flow and leeward sides of the cone, the boundary layer development follows a similar way, with only quantitative difference on $\ell_0^+$.

Figures 6 and 7 show the streamwise evolvements of the Reynolds shear stress and streamwise mean velocity profiles during the transition process of case GAC-0. At the transition onset the mean velocity is of a laminar profile (Fig. 7) and the Reynolds shear stress is very small (Fig. 6). After that the boundary layer evolves rapidly from a wall-normally Blasius structure to a four-layer TBL structure, as displayed in Fig. 7. A detailed observation of the variation of the mean velocity profile indicates that the near-wall viscous sublayer and buffer layer form before the outer layer, which is reasonable. This streamwise development is currently described by a growth of $\ell_0^+$ and $y_{buf}^+$ only, as shown in Fig. 5. Although the true establishment of the TrBL may be more complicated, the current proposal is tested to be a good approximation, as comparisons show. At the location with the peak heat flux, the transition has almost been completed: the van Driest-transformed mean velocity profile is close to a standard four-layer TBL shape, and collapses in the log-layer with the logarithmic law of incompressible TBL (Fig. 7). Moreover, the Reynolds shear stress profiles become invariant in the inner region in wall unit, and in the outer region with the outer coordinate, both agreeing with the DNS of Pirozzoli et al. for a flat-plate TBL at $Ma = 2.25$ [31] (Fig. 6), showing the similarity of the flat-plate TBL and the cone TBL (at zero incidence). Therefore, the *Re*- and *Ma*-invariance

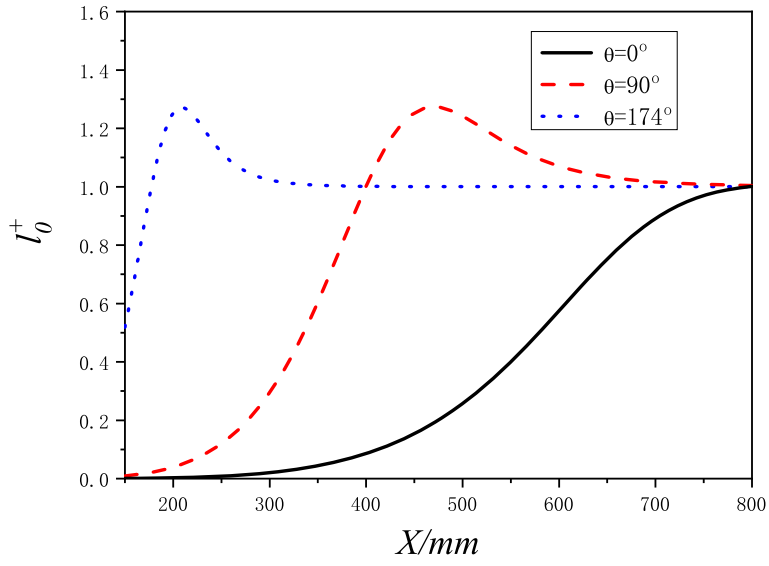


(a)

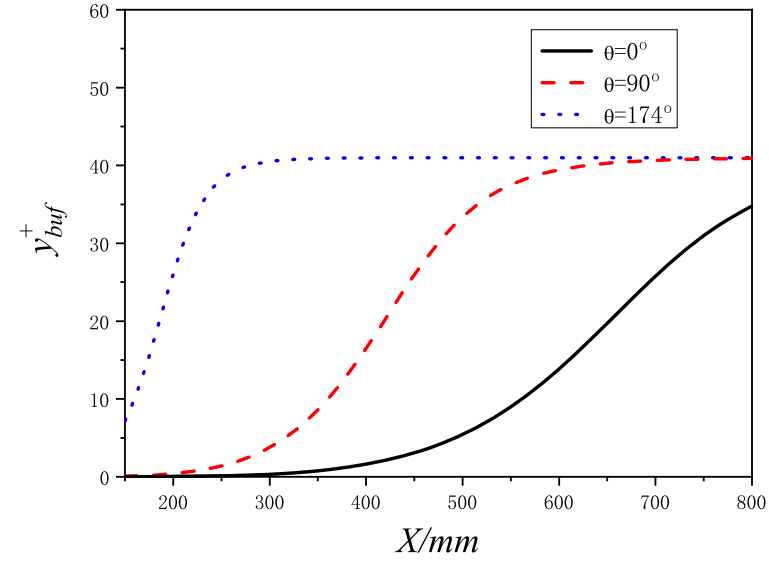


(b)

**Fig. 5** Evolution of **a** the near wall eddy length $\ell_0^+$ and **b** the buffer layer thickness $y_{buf}^+$ along different meridian lines for the GAC-6 case

properties of the Reynolds stress in the TBL regime are correctly captured by the SED-SL model.

### 3.2 Simulation of the CARDC experiment

The measurement conducted by Chen et al. in CARDC [23] is a very recent experimental study about the hypersonic transitional flow on a sharp cone. The data are of high accuracy, high resolution, and high repeatability. However, only $\Delta T_w$ data are provided, and

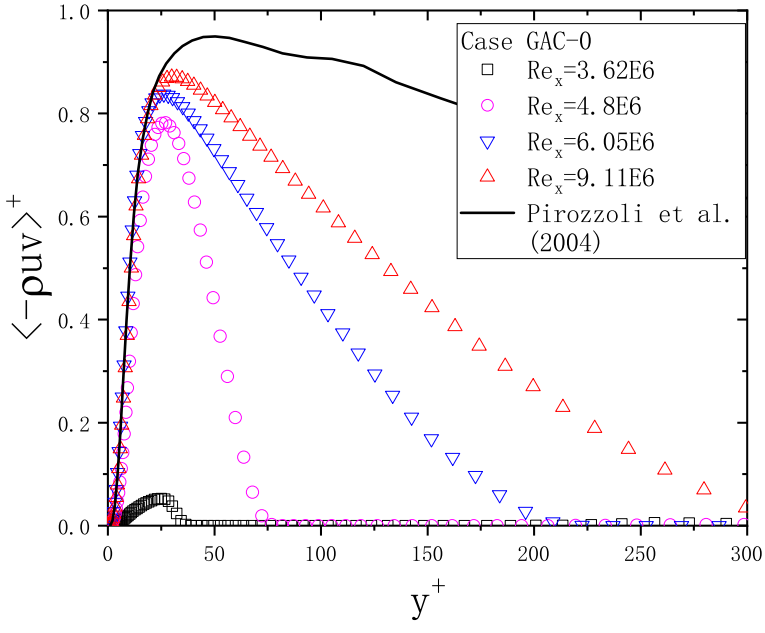


(a)

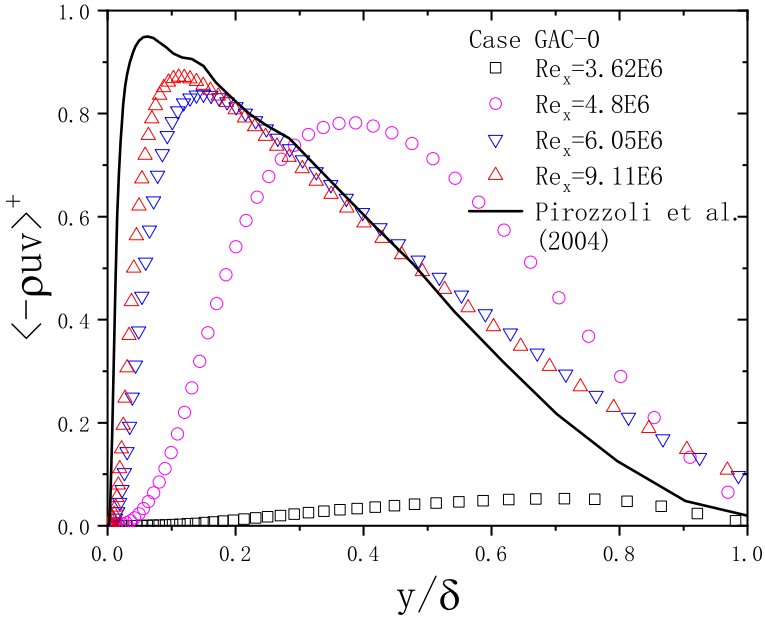


(b)

**Fig. 6** The Reynolds shear stress profiles at four streamwise locations for the GAC-0 case, plotted in **a** the inner coordinate and **b** the outer coordinate. $Re_x = 3.62E6$ indicates the transition onset location and $Re_x = 6.05E6$ indicates the transition peak location. Solid line denotes the DNS data of Pirozzoli et al. for an adiabatic flat-plate TBL at $Ma = 2.25$ [31]

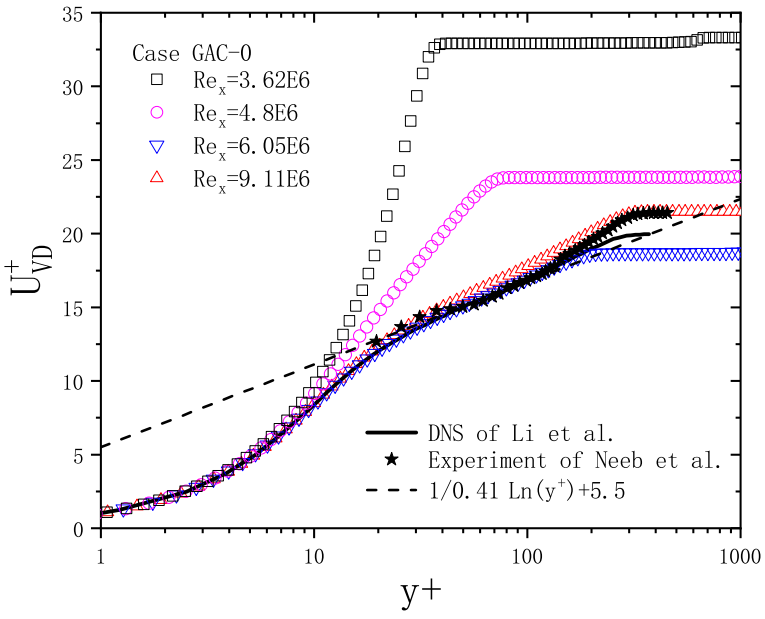


**Fig. 7** The van Driest transformed streamwise mean velocity profiles at four streamwise locations for the GAC-0 case. Solid stars denote the experimental data of Neeb et al. for TBL over a 7° half angle cone at $Ma = 6$ [32]. Solid line denotes the DNS data of Li et al. for TBL over a 10° half angle cone at $Ma = 0.7$ [33]

the measurement is restricted to the windward and leeward sides of the cone, making the cross-flow regime inaccurate owing to the large angle of view. Here, we present the computation of the CARDC cases with the SED-SL model.

The settings of the model parameters for the CARDC cases are shown in Fig. 1. Because $\Delta T_w$ is closely correlated with the surface heat flux as revealed by Fig. 2, we directly compare the simulated $St$ with the rescaled $\Delta T_w$, in which the proportional factor is determined by making the laminar data collapse together.

Figure 8 compares the $\Delta T_w$ contours with the SED-SL computed $St$ contours for all the four CARDC cases. For the cones with nonzero $AoA$, the windward and leeward surfaces are compared separately. The agreement between the simulation and measurement is excellent throughout the cone surface and for all test cases. Therefore, the current model demonstrates a high accuracy and a wide adaptivity in describing various hypersonic TrBLs.

Further comparisons on profiles are performed in Figs. 9, 10, 11 and 12 for each CARDC case, which confirm the agreements of the contours. In Fig. 9, specifically, the $St$ profile along the cone axial direction computed by the SED-SL is compared with the rescaled $\Delta T_w$ profile measured in the experiment for the CARDC-0 case. Also plotted in Fig. 9 is the GAC-0 case, to evaluate the similarity and discrepancy between the two experiments. One finds that the SED-SL model accurately describes the surface heat transfer properties of both TrBLs. A major difference between the two flows is the transition onset location, which is earlier in the CARDC-0 case. Besides the small discrepancy on $Ma$, two reasons might contribute to this difference. First, the nose-tip radii of the GAC cone is much larger than that of the CARDC one, leading to a postponed transition onset for the GAC-0 case according to [5]. Second, the free-stream noise level characterized by $Tu = p_{rms}/p$ is

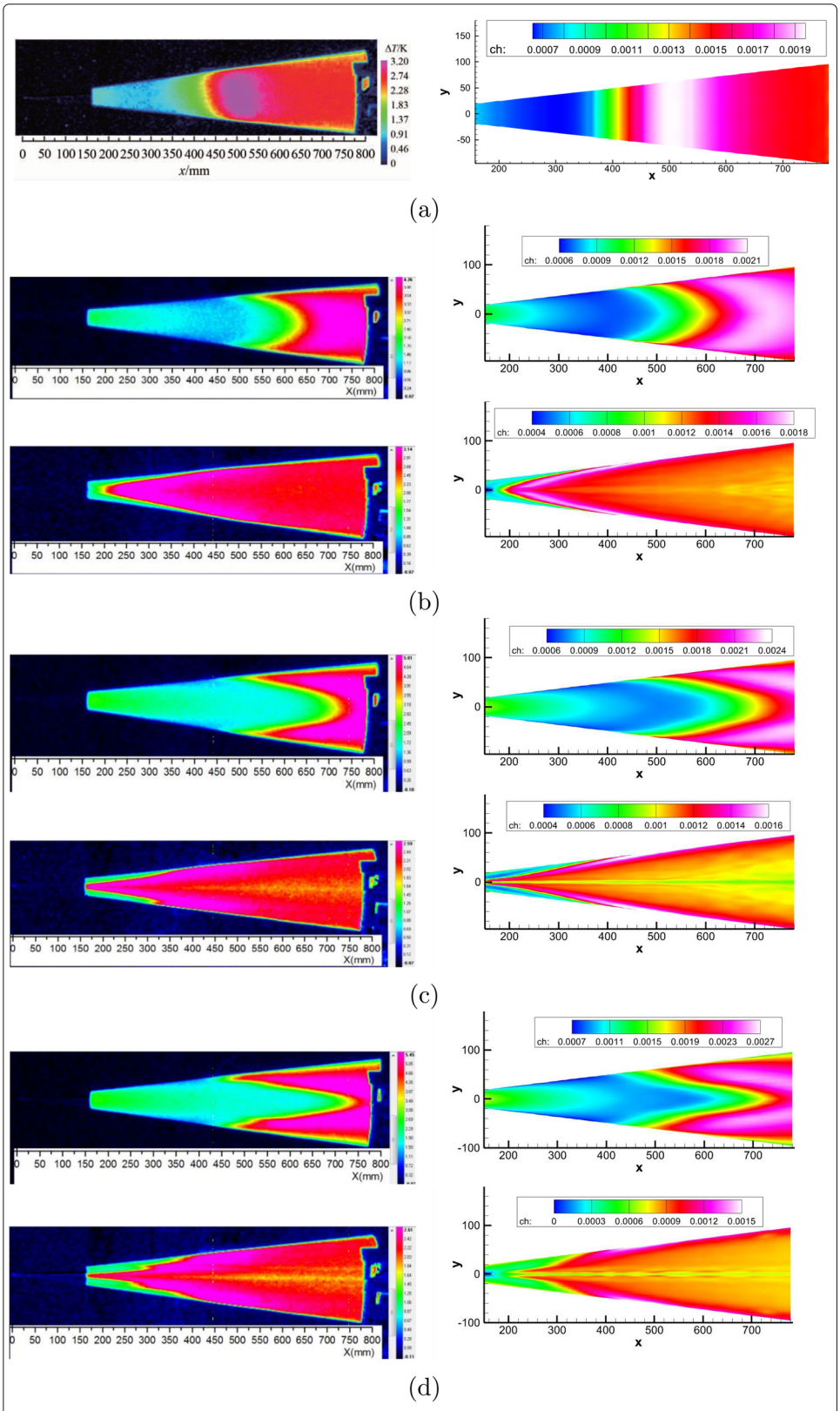


**Fig. 8** Comparisons between the surface temperature increment contours measured in experiment [23] and the *St* contours computed by the SED-SL model for **a** the CARDC-0 case, and the windward and leeward surfaces of **b** the CARDC-2 case, **c** the CARDC-4 case, and **d** the CARDC-6 case

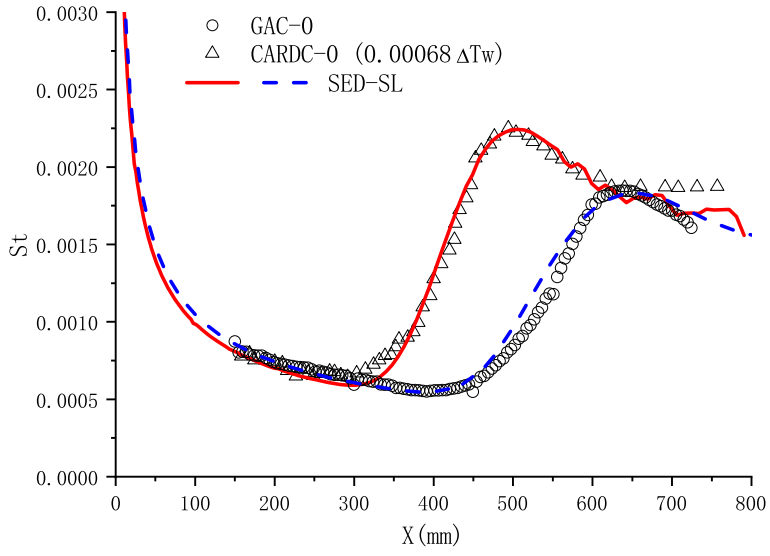


**Fig. 9** The *St* distributions along the meridian line computed by the SED-SL model for the GAC-0 and CARDC-0 cases, compared with the experimental data. For the CARDC-0 case, the experimental data are the rescaled surface temperature increments

about 3.9% for the CARDC-0 case according to [23], and that of the GAC-0 case is about 2%, which also results in an earlier transition for the CARDC-0 flow [34]. Other than the transition onsets, the two transitional flows are almost identical in the laminar and fully turbulent regimes, which is captured by the SED-SL model.

## 4 Discussion and conclusion

In this work the HBL transition on a slender cone at moderate incidence has been studied via a symmetry-based length model: the SED-SL model. It is shown that, by properly setting the multi-regime structure of the TrBL through only three parameters (i.e. a transition center, an after-transition near-wall eddy length, and a transition width quantifying transition overshoot), the SED-SL correctly reproduces the heat flux distribution on the whole cone surface (from windward to leeward side), agreeing closely with multiple sets of wind tunnel data. The results demonstrate the validity of the SED theory regarding the multi-regime similarity across a non-equilibrium transitional process. The success indicates that a universal feature of the TrBL is captured, which is an organizational principle for TBL (due to wall dilation symmetry), and then yields a simple algebraic model for transitional HBLs.

The current SED-SL model has three distinct features compared to popular RANS models: its simplicity, accuracy and transparency for its parameter interpretation. The goal of this paper is not yet to conclude a matured transition model for industrial application, but to validate the symmetry-based description of the transitional HBLs. The current success indicates that, with the accumulation of validated flow cases, a practical transition model will emerge for computing a considerably large number of flows, with both high prediction accuracy and wide adaptivity.

Note that the "similarity structure" proposed by the SED theory is statistical, and is distinct from those highly unstable patterns such as instantaneous vortex structures or

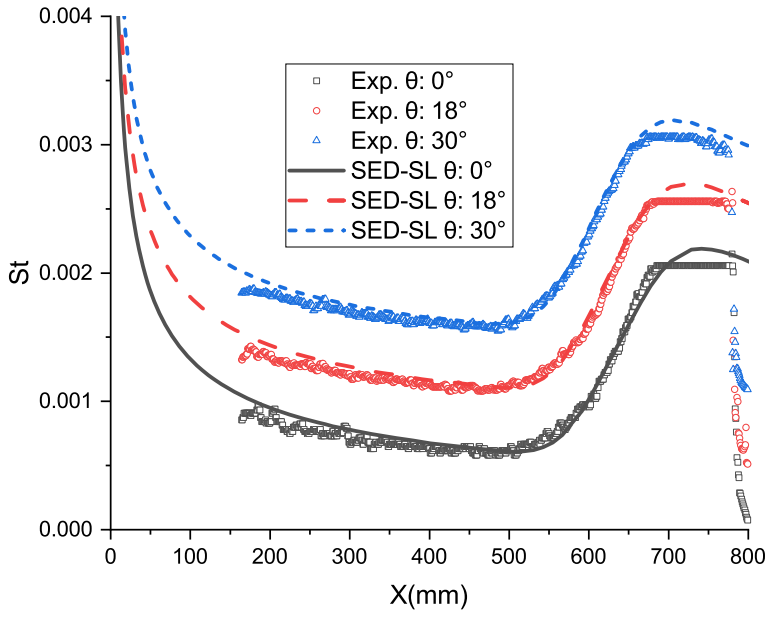


(a)

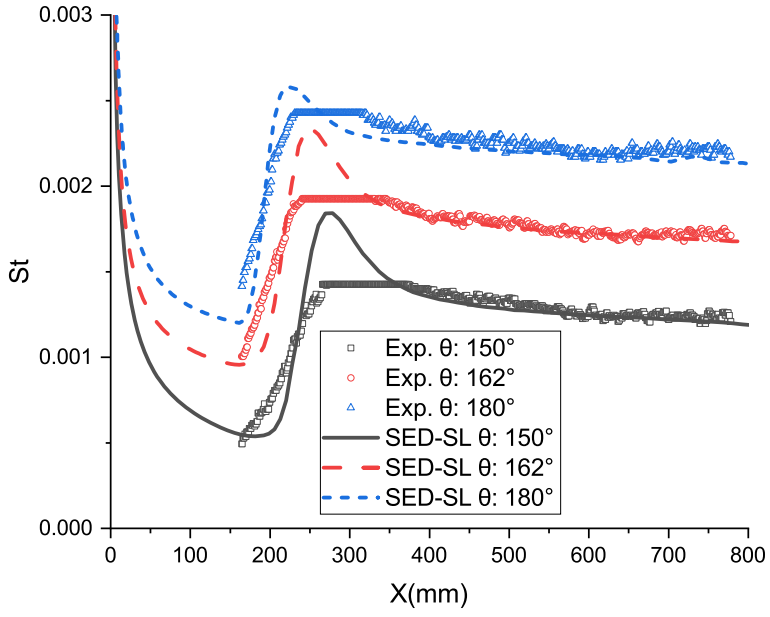


(b)

**Fig. 10** Comparisons between the rescaled surface temperature increment distributions measured in experiment and the *St* distributions computed by the SED-SL model for the CARDC-2 case. **a** The windward surface, **b** the leeward surface. The data are vertically translated to be clearly displayed

wave-like perturbations (which have been the targets in the stability theory and coherent structure studies). But we assert that only the similarity structure is stable and can be directly related to mean flow properties (such as skin friction), so as to be relevant to

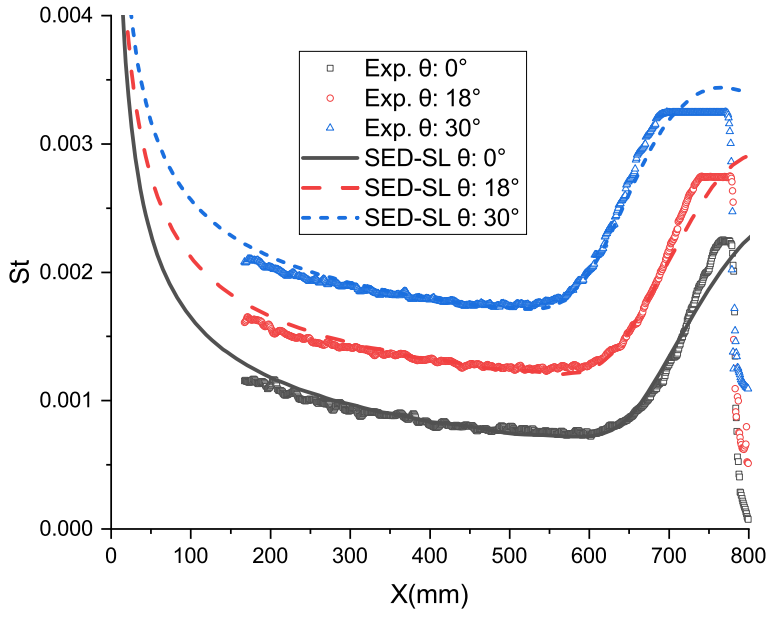


**Fig. 11** Comparisons between the rescaled surface temperature increment distributions measured in experiment and the *St* distributions computed by the SED-SL model for the CARDC-4 case. **a** The windward surface, **b** the leeward surface. The data are vertically translated to be clearly displayed

engineers' prediction ability. So, the present results further support the assertion that the most important task in the basic study of engineering flows is to characterize and quantify this similarity structure.

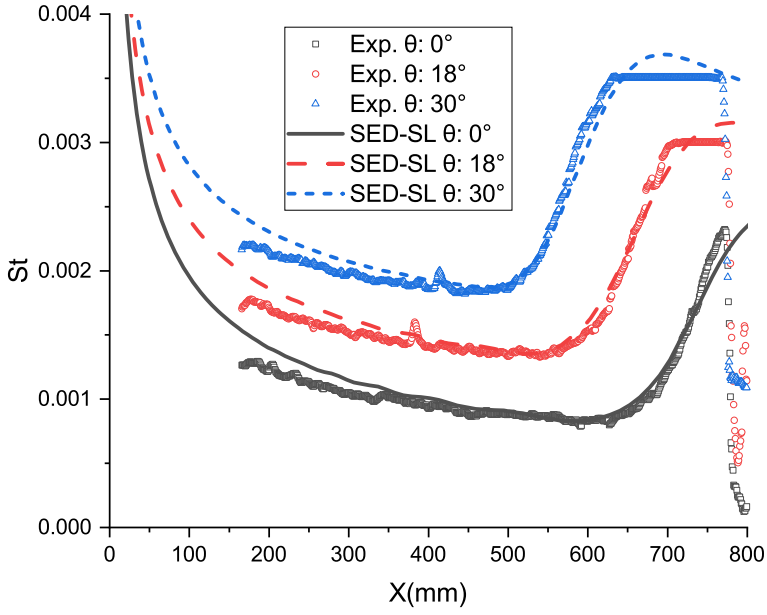


**Fig. 12** Comparisons between the rescaled surface temperature increment distributions measured in experiment and the *St* distributions computed by the SED-SL model for the CARDC-6 case. **a** The windward surface, **b** the leeward surface. The data are vertically translated to be clearly displayed

For future perspective, it would be intriguing to investigate the dependence of the transition-relevant multi-regime structure parameters on various flow parameters. For example, our preliminary study shows that $\ell_0^\infty$ decreases with increasing *Ma*, which is sound as compressibility yields a "compression" of eddy size globally, hence a smaller

eddy-viscosity. Another crucial transition parameter is the transition center $x^*$, which defines the transition location that is of utmost importance in aerospace engineering. New correlation relationships between $Re_{x^*}$ and multiple transition influential factors have to be established for the current SED-SL model to reach full predictability, which we will demonstrate to be feasible in a future communication, since we have captured the right similarity structure.

**Acknowledgements**
The authors thank Dr. M.-J. Xiao for her contribution to the SED-SL model.

**Authors' contributions**
W.-T. Bi: Analysis, Writing original draft. Z. Wei and K.-X. Zheng: Simulation, Analysis. Z.-S. She: Methodology, Supervision, Funding acquisition, Writing, Reviewing and Editing. All authors read and approved the final manuscript.

**Authors' information**
W.-T. Bi
Research Scientist.
Z. Wei and K.-X. Zheng
PhD candidate.
Z.-S. She
Professor.

**Funding**
This material is based upon work supported by the NNW Project, the Open Project of Science and Technology on Scramjet Laboratory, and the NNSF of China under Grant Number 91952201,11372008,11452002.

**Availability of data and materials**
The numerical simulation data will be available for others to download.

## Declarations

**Competing interests**
The authors declare that they have no competing interests.

**Author details**
[1]State Key Laboratory for Turbulence and Complex Systems and Department of Mechanics and Engineering Science, College of Engineering, Peking University, Beijing 100871, China. [2]Science and Technology on Scramjet Laboratory, China Aerodynamics Research and Development Center, Mianyang 621000, China. [3]State Key Laboratory of Aerodynamics, China Aerodynamics Research and Development Center, Mianyang 621000, China. [4]Computational Aerodynamics Institute, China Aerodynamics Research and Development Center, Mianyang 621000, China.

Received: 22 January 2022 Accepted: 28 April 2022
Published online: 08 July 2022

**References**

1. Chen JQ, Yi SH, Li XL, Han GL, Zhang YF, Yang Q, Yuan XX (2021) Theoretical, numerical and experimental study of hypersonic boundary layer transition: Blunt circular cone. Appl Therm Eng 194:116931
2. Schneider SP (2004) Hypersonic laminar-turbulent transition on circular cones and scramjet forebodies. Prog Aerosp Sci 40:1–50
3. Lee C-B, Jiang X-Y (2019) Flow structures in transitional and turbulent boundary layers. Phys Fluids 31:111301
4. Anderson JD (1989) Hypersonic and high temperature gas dynamics. McGraw-Hill Book Company (UK) Ltd., Maidenhead
5. Paredes P, Choudhari MM, Li F, Jewell JS, Kimmel RL, Marineau EC, Grossir G (2019) Nose-tip bluntness effects on transition at hypersonic speeds. J Spacecr Rockets 56:369–387
6. Menter FR, Langtry R, Vlker S (2006) Transition modelling for general purpose CFD codes. Flow Turbul Combust 77:31–48
7. Menter FR, Smirnov PE, Liu T, Ravikanth A (2015) A one-equation local correlation-based transition model. Flow Turbul Combust 95:583–619
8. Savill AM (1993) Evaluating turbulence model predictions of transition. Appl Sci Res 51:555–562
9. Durbin PA (2018) Some recent developments in turbulence closure modeling. Annu Rev Fluid Mech 50:77–103
10. Wan BB, Tu GH, Yuan XX, Chen JQ, Zhang YF (2021) Identification of traveling crossflow waves under real hypersonic flight conditions. Phys Fluids 33:044110
11. Li XH, Chen JQ, Huang ZF, Yang Q, Xu GL (2020) Stability analysis and transition prediction of streamwise vortices over a yawed cone at Mach 6. Phys Fluid 32:124110
12. Wang L, Fu S (2009) Modelling flow transition in a hypersonic boundary layer with Reynolds-averaged Navier-Stokes approach. Sci China Phys Mech Astron 52:768–774
13. Liu ZJ, Yan C, Cai FJ, Yu J, Lu YH (2020) An improved local correlation-based intermittency transition model appropriate for high-speed flow heat transfer. Aerosp Sci Technol 106:116122

14. She ZS, Chen X, Hussain F (2017) Quantifying wall turbulence via a symmetry approach: a Lie group theory. J Fluid Mech 827:322–356
15. Chen X, Hussain F, She ZS (2018) Quantifying wall turbulence via a symmetry approach. part 2. Reynolds stresses. J Fluid Mech 850:401–438
16. Chen X, Hussain F, She Z-S (2019) Non-universal scaling transition of momentum cascade in wall turbulence. J Fluid Mech 871:R2
17. She ZS, Zou HY, Xiao MJ, Chen X, Hussain F (2018) Prediction of compressible turbulent boundary layer via a symmetry-based length model. J Fluid Mech 857:449–468
18. Xiao MJ, She ZS (2019) Symmetry-based description of laminar–turbulent transition. Sci China Phys Mech Astron 62:994711
19. Xiao MJ, She ZS (2020) Precise drag prediction of airfoil flows by a new algebraic model. Acta Mech Sin 36:35–43
20. Prandtl L (1925) Uber die ausgebildete turbulenz. ZAMM 5:136–139
21. Baldwin B, Lomax H (1978) Thin-layer approximation and algebraic model for separated turbulent flows. AIAA 1978-257, Paper presented at the 16th Aerospace Sciences Meeting, Huntsville, 16-18 January 1978. https://doi.org/10.2514/6.1978-257
22. Willems S, Gulhan A, Juliano TJ, Schneider SP (2014) Laminar to turbulent transition on the HIFiRE-1 cone at Mach 7 and high angle of attack. AIAA 2014-0428, Paper presented at the 52nd Aerospace Sciences Meeting, National Harbor, 13-17 January 2014. https://doi.org/10.2514/6.2014-0428
23. Chen JF, Ling G, Zhang QH, Xie FT, Xu XB, Zhang YF (2020) Infrared thermography experiments of hypersonic boundary-layer transition on a 7 degree half-angle sharp cone. J Exp Fluid Mech 34:60–66
24. Franko KJ, Lele SK (2013) Breakdown mechanisms and heat transfer overshoot in hypersonic zero pressure gradient boundary layers. J Fluid Mech 730:491–532
25. Grossir G, Pinna F, Bonucci G, Regert T, Rambaud P, Chazot O (2014) Hypersonic boundary layer transition on a 7 degree half-angle cone at Mach 10. AIAA 2014-2779, Paper presented at the 7th AIAA Theoretical Fluid Mechanics Conference, Atlanta, 16-20 June 2014. https://doi.org/10.2514/6.2014-2779
26. Casper KM, Johnson HB, Schneider SP (2011) Effect of freestream noise on roughness-induced transition for a slender cone. J Spacecr Rockets 48:406–413
27. Sivasubramanian J, Fasel HF (2015) Direct numerical simulation of transition in a sharp cone boundary layer at Mach 6: fundamental breakdown. J Fluid Mech 768:175–218
28. Zhu YD, Chen X, Wu JZ, Chen SY, Lee CB, Gad-el-Hak M (2018) Aerodynamic heating in transitional hypersonic boundary layers: Role of second-mode instability. Phys Fluids 30:011701
29. Qin YP, Yan C, Zhao ZH, Wang JJ (2018) An intermittency factor weighted laminar kinetic energy transition model for heat transfer overshoot prediction. Int J Heat Mass Transf 117:1115–1124
30. Wu XH, Moin P, Wallace JM, Skarda J, Duran AL, Hickev JP (2017) Transitional-turbulent spots and turbulent-turbulent spots in boundary layers. PNAS 114:5292–5299
31. Pirozzoli S, Grasso F, Gatski TB (2004) Direct numerical simulation and analysis of a spatially evolving supersonic turbulent boundary layer at M=2.25. Phys Fluids 16(3):530–545
32. Neeb D, Saile D, Gulhan A (2018) Experiments on a smooth wall hypersonic boundary layer at Mach 6. Exp Fuids 68:1–21
33. Li XL, Fu DX, Ma YW (2008) DNS of compressible turbulent boundary layer around a sharp cone. Sci China Ser G Phys Mech Astron 51:699–714
34. Schneider SP (2001) Effects of high-speed tunnel noise on laminar-turbulent transition. J Spacecr Rocket 38:323–333


## Publisher's Note